A Polydisperse Polymer Solution as a Critical System

Shelly Livne

Department of Materials and Interfaces, Weizmann Institute of Science, Rehovot 76100, Israel

Received September 29, 1993; Revised Manuscript Received January 12, 1994®

ABSTRACT: Polydisperse solutions of polymers, formed by a reversible polymerization process, are studied by computer simulation. The system is described by a stepwise elongation and contraction process which is based on adding (or deleting) one link to a chain end. In such a process, cyclic polymers cannot be formed. The growth of a polymer is controlled by two chemical potentials that determine the number of polymers and their length and, hence, the concentration of the system. Such a reversible polymerization process can be described by a magnetic analog of the n-vector model. Thus, this system can be used to emphasize the correspondence between polymer models and critical magnetic models. The entire phase space of concentrations of a polydisperse solution is studied. We describe the long range of validity of the semidilute regime, in which the polymer chains are only slightly overlapping. Our results also indicate that, basically, a polydisperse solution shows the same behavior as a monodisperse one. In the limit of dense chains, we study the hypothesis that the system is controlled by one "infinite" chain that leads to a transition toward a collapsed phase. We performed several studies in this regime and found no evidence for an infinite chain nor for a collapsed phase.

I. Introduction

There are a number of systems in which polymerization is believed to take place under conditions of chemical equilibrium between the polymers and their respective monomers. If the polymerization requires the presence of an initiator and commences in a defined direction, the polymers constructed are open chains, and the system does not contain rings. Examples include the polymerization of "living polymers",[1] such as poly-α-methylstyrene and polytetrahydrofuran, which, under appropriate conditions, create long linear polymer-like micelles. A cylindrical microemulsion composed of water, oil, and surfactant, under certain conditions, can also form such a polymer-like phase.[2] This phenomenon is also found in some biological systems, such as actin and tubulin, which polymerize from protein subunits to form the skeleton of a living cell.[3]

Our understanding of the statistical mechanics of such systems comes, to a large extent, from the study of simple, idealized models of interacting chains. One of the widely studied models was derived from the n-vector model of magnetism. The formal analogy between polymers and magnetic systems was first pointed out by de Gennes,[4] who made the remarkable observation that the properties of a self-avoiding walk (SAW) can be mapped onto the $n \rightarrow 0$ limit of an n-component field theory. The idea was further extended by des Cloizeaux,[5] to describe polymers in a solution. In equilibrium, the polymers are polydispersed, with a wide chain length distribution that is controlled by two fugacities. The phase space of concentration, which is spanned by these two fugacities, can be crudely divided into three regions.

(1) The dilute region, in which the chains do not interact, can be regarded as a grandcanonical distribution of a single SAW. This observation was verified by both theoretical[6,7] and numerical studies.[8]

(2) In the semidilute regime, it is interesting to compare the properties of a polydisperse system with those of a monodisperse one. Using ϵ expansion calculations, Schäfer *et al.*[9] concluded that qualitative properties (i.e. critical exponents) are not influenced by polydispersity. However, quantitative results, such as scaling functions, are influenced.

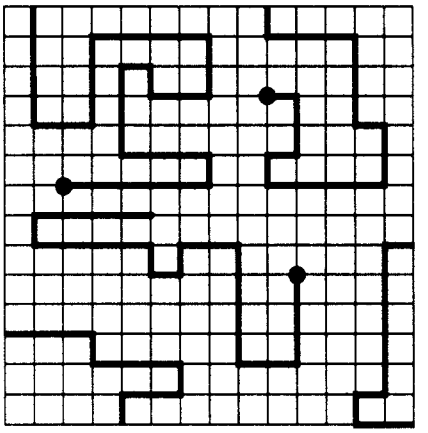

Figure 1. A two-dimensional scheme of a sample configuration of the SEC process on a portion of the square lattice. The filled circles represennt active chain ends.

(3) In the dense chains limit, where screening effects cause the chains to become ideal, the system resembles a polymer melt.[7,10] This observation was questioned by Gujrati[6] who has developed a direct scaling approach to describe polydispersity. His approach has made a unique contribution to the high concentrations limit. In contradiction to other studies,[7,10] Gujrati argued that, below a certain line in the system's phase diagram, the polymers are collapsed, and the system forms a new phase. This theory predicts the existence of an "infinite" chain, for which new scaling relations can be derived. In order to establish which of the above predictions provides a better description for the dense phase of a polydisperse solution, direct numerical techniques, such as computer simulation, are required.

We present here an efficient simulation technique for studying the reversible polymerizing system, which is defined by a grand function with two fugacities. This technique can be regarded as a direct extension of two methods: the stepwise dynamics of critical Ising clusters[11] and the Berretti and Sokal algorithm, which was confined to the problem of a single SAW.[8] Our technique is capable of simulating the entire phase space spanned by the two fugacities, which corresponds to a large range of concentrations.

® Abstract published in *Advance ACS Abstracts,* August 15, 1994.

0024-9297/94/2227-5318$04.50/0 © 1994 American Chemical Society

II. The Stepwise Elongation and Contraction Method

The proposed method is a dynamical Monte Carlo process for a solution of polymer chains. The chains undergo a stepwise elongation and contraction (SEC) with a fugacity, λ, for adding (or deleting) a chain-end link. The number of chains in the system is controlled by another fugacity, η, for chain ends. In this process a grand canonical ensemble of chain lengths is formed. A representative configuration of the SEC procedure is shown in Figure 1.

Since the SEC process is conducted over chain ends only, it follows that a chain cannot break in the middle and, also, that two chains cannot aggregate. Therefore, no rings are formed. Moreover, since the polymerization requires an initiator, we assume that only one end of each chain is an active tip, from which the chain is growing and contracting. Thus, the partition function of the system is given by

$$\Xi = \sum_{p=1}^{\infty} \sum_{l>p}^{\infty} \eta^p \lambda^l U_{l,p} \tag{1}$$

where $U_{l,p}$ is the number of ways to arrange p different SAWs of total number of links l on a lattice of N_0 sites (N_0, which is the volume of the system, is kept fixed).

The concentration of links Φ_l ($=l/N_0$), and that of polymers Φ_p ($= p/N_0$), can be defined using the standard relation between concentrations and activities

$$\Phi_l = \frac{1}{N_0} \frac{\partial \ln \Xi}{\partial \ln \lambda} \tag{2}$$

$$\Phi_p = \frac{1}{N_0} \frac{\partial \ln \Xi}{\partial \ln \eta} \tag{3}$$

and the averaged polymer length is

$$\langle N \rangle = \frac{\Phi_l}{\Phi_p} \tag{4}$$

Equation 1 resembles the partition function of the $n = 0$ vector model with external magnetic field H. In this analogy, $H = \eta^{1/2}$ and $J = \lambda$ (J is the nearest-neighbor coupling constant). Since Ξ cannot be solved directly, it is useful to consider the magnetic analog, for which it is possible to obtain[12,13]

$$\Phi_l = \epsilon^{d\nu-1} f_l(x) \tag{5}$$

$$\Phi_p = \epsilon^{d\nu} f_p(x) \tag{6}$$

$$\langle N \rangle = \epsilon^{-1} \frac{f_l(x)}{f_p(x)} \tag{7}$$

where d is the dimensionality of the system, $x = M/\epsilon^{\beta}$ (M is the magnetization), ν and β are the standard critical exponents, and $\epsilon = (T_c - T)/T_c$.

In this analogy $T_c \leftrightarrow \lambda_c$. Thus, it is possible to define the approach toward the critical limit as

$$\epsilon \equiv \frac{\lambda_c - \lambda}{\lambda_c} \tag{8}$$

For $\lambda > \lambda_c$ ($T < T_c$), we will use $|\epsilon|$. The critical value of the reversible polymerization system is obtained for $\lambda_c \equiv 1/\mu$, where μ is the effective coordination number of the lattice. In this limit, the growth of an infinitely large chain is exactly in balance with the excluded volume restriction.

The stochastic algorithm is described as follows. We start from an empty lattice filled with "solvent" monomers. At each Monte Carlo (MC) step, either a dimer is formed from two adjacent monomers or a monomer is added or deleted from a chain end. The transition probabilities are

$$P_d = \frac{n_d \eta}{n_d \eta + n_e}$$

$$P(N \rightarrow N+1) = \frac{z\lambda}{1 + z\lambda} \frac{n_e}{(n_d \eta + n_e)}$$

$$P(N \rightarrow N-1) = \frac{1}{1 + z\lambda} \frac{n_e}{(n_d \eta + n_e)} \tag{9}$$

where P_d is the probability to form a dimer, n_d is the number of empty locations, n_e is the number of chain ends, and z is the coordination number of the lattice. A random number is chosen between zero and one and is compared to the transition probabilities of eq 9, where three possibilities can occur: (1) If the random number is less than P_d, a random site is chosen from the list n_d, and a new dimer, which starts a new chain, is located. (2) If the random number is larger than P_d but less then the sum $P_d + P(N \rightarrow N+1)$, one chain end is chosen from the list n_e and a direction is chosen at random and checked for self-avoidance; if it is self-intersecting, then the attempted move is rejected, and the old configuration is counted again in the sample. If the self-restriction is obeyed, a new link is added to the chain. (3) Since the probabilities of eq 9 are normalized to one, the last possibility is to remove one link from one of the chains. Such a chain is chosen at random from the n_e list, and the last link at the end of the chain is removed. If the chain chosen consists of a single link, the chain is discarded from the lattice.

This SEC algorithm resembles that of Bereti and Sokal (BS), which was suggested for a single SAW.[8] Similarly to the BS algorithm, the SEC algorithm is ergodic; i.e. it is possible to obtain any configuration w' from any w by a finite sequence of allowed moves. This can be easily shown. One simply uses the $N \rightarrow N - 1$ moves to remove all the chains of configuration w and then uses the $N \rightarrow N + 1$ moves to build up step-by-step the configuration w'.

Our SEC process is, crudely speaking, a random walk process, and the average time required to go from a walk of N monomers to a one monomer walk is of order N^2. But each time the one monomer walk is reached, all memory of the past is lost, and future walks are then independent of the past ones. Thus, in order to obtain an uncorrelated configuration, one has to make $\tau \sim \langle N \rangle^2$ MC steps. The thermodynamic limit is obtained for $\epsilon \rightarrow 0$ which causes $\langle N \rangle \rightarrow \infty$. However, for small ϵ, τ also becomes infinite, which makes the simulation inefficient.

III. Results and Discussion

The SEC algorithm is performed in two systems: a two-dimensional (2d) and a 3-dimensional (3d) system which were simulated by the square lattice and the cubic lattice, respectively. Periodic boundary conditions were assumed in most of the calculations, except for the first test, where we were interested in finite size effects due to the lattice "walls" and used reflecting boundary conditions.

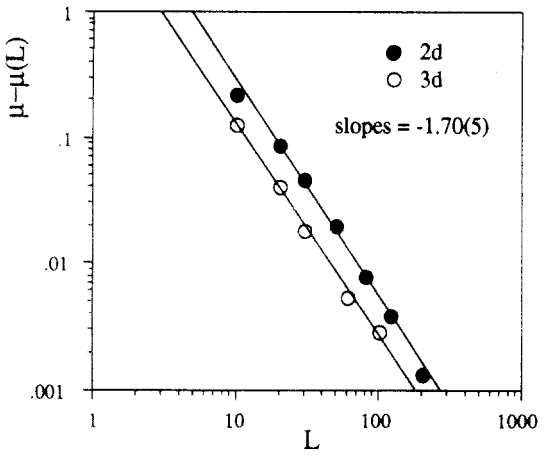

Figure 2. log–log plot of the deviation from μ vs the lattice size L. The data scales in agreement with eq 12.

In order to obtain a polymer system in the thermodynamic limit (long chains), we chose $\eta \ll \lambda$. The control over the two fugacities produces a solution of variable concentrations. The dilute limit is defined for $\lambda < \lambda_c$, (with $\lambda_c(3d) = 0.213$ and $\lambda_c(2d) = 0.379$), while for $\lambda > \lambda_c$ the chains are mutually interacting. In each of these concentration regimes, we performed a separate MC experiment. A single experiment starts from an empty lattice, and the first 10^6 MC moves are not counted. Then, an additional 10^8 MC moves are performed, with three iteration in between. In order to establish the number of MC moves needed to equilibrate the system, we carried out a test run. In this test, we started from a lattice filled with rod-like polymers, with Φ_l of $\approx$0.35, which is the highest concentration studied, and the system was allowed to equilibrate. This test system was compared to another system, in which the starting configuration was an empty lattice, and we chose λ and η which produce $\approx$0.35 link density. We counted the number of configurations needed in order that the two runs will produce the same "equilibrium" behavior. This number was used for simulations of lower concentrations as well, although a lower concentration needs fewer MC moves in order to reach equilibrium.

A. Finite Size Effects. In a finite system, the size of the chains constructed cannot exceed the lattice size. Thus, the average number of segments in each chain is proportional to L, the linear size of the lattice. The effective coordination number of the lattice, $\mu(L)$, is less than the asymptotic value μ. In the dilute limit where $\lambda < \lambda_c$, for $\eta \to 0$, effectively only a single chain is simulated, and finite size effects due to the lattice "walls" are important. We define an excluded volume interaction between monomers of the chain and the "walls" of the lattice, and we control λ, such that $P(N \to N+1)$ is sufficiently large to overcome the excess excluded volume and to obey reversibility:

$$P(N \to N-1) = P(N \to N+1)[1 - b(L)] \tag{10}$$

where $b(L)$ is the average excluded volume per site in a lattice of size L. Using eq 9, $\mu(L)$ is obtained by

$$\mu(L) = z[1 - b(L)] \tag{11}$$

which should scale as

$$\mu(L) = \mu\left[1 - \frac{c}{L^y}\right] \tag{12}$$

In Figure 2 we have plotted $[\mu - \mu(L)]$ vs L on a log–log scale, and from the slopes the scaling exponent $y = 1.7$ is obtained, in both 2d and 3d systems. Due to this large y, for lattice sizes larger than $L = 100$, the asymptotic behavior of an unrestricted SAW is already obtained. The estimation of x provides a check for finite size effects due to the lattice.

A direct measure of the configuration of the polymers is the average squared radius of gyration, $\langle R_g^2 \rangle$, and the average number of segments in a polymer, $\langle N \rangle$, as functions of L. Using a standard summation method for critical clusters,[14] we calculate

$$\langle R_g^2 \rangle = \left\langle \frac{\sum_i R_{gi}^2 N_i^2}{\sum_i N_i^2} \right\rangle \tag{13}$$

where N_i is the number of monomers of the ith cluster, R_{gi} is the cluster gyration radius, and the summation is carried over all the clusters in the lattice. The brackets $\langle\ \rangle$ represent a statistical mean over all sample configurations. Similarly,

$$\langle N \rangle = \left\langle \frac{\sum_i N_i^2}{\sum_i N_i} \right\rangle \tag{14}$$

In this study, we are using periodic boundary conditions, $\lambda = \lambda_c$, and a very small η. Thus, on average, a single chain is constructed. If a chain had been constructed on an infinite lattice, using the asymptotic value λ_c, we would have expected that $\langle N \rangle$ would go to infinity and we would obtain the behavior of a SAW. Here, however, the chain growth is controlled by the limited volume of the lattice. Therefore, we still expect a SAW behavior, with a gyration

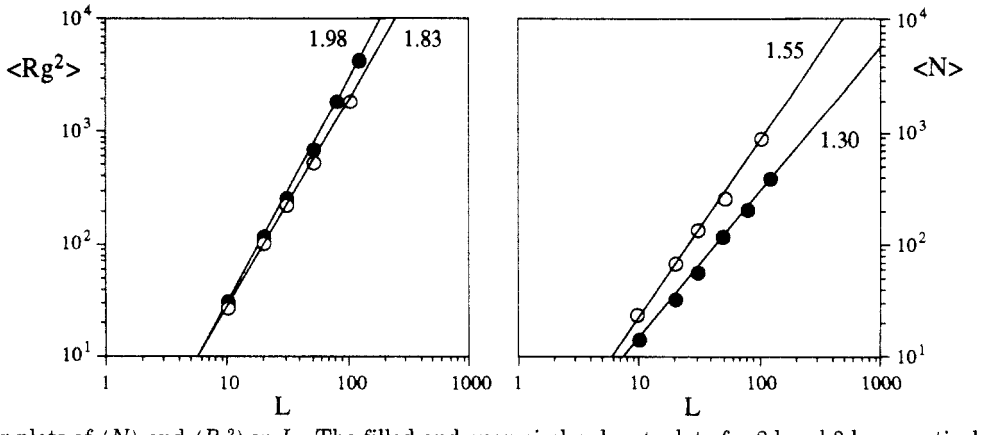

Figure 3. log–log plots of $\langle N \rangle$ and $\langle R_g^2 \rangle$ vs L. The filled and open circles denote data for 2d and 3d, respectively. Here, $\eta = 10^{-13}$ and $\epsilon = 0$ (i.e. $\lambda = \lambda_c$).

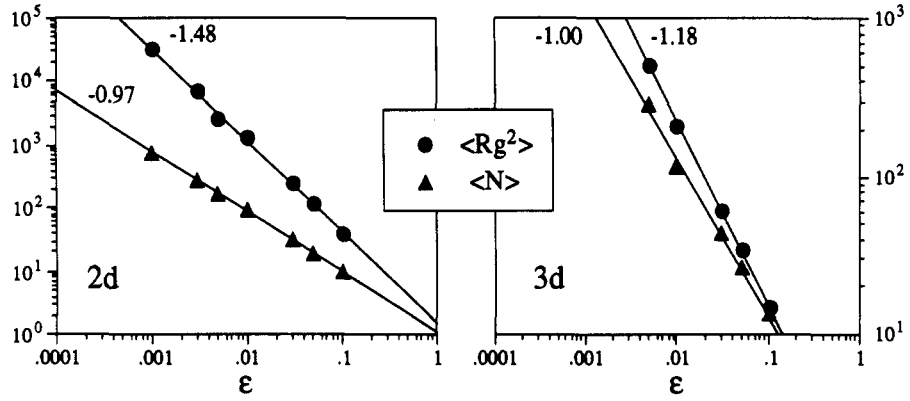

Figure 4. log–log plot of $\langle N\rangle$ and $\langle R_g^2\rangle$ vs ϵ. The data were obtained for the region $\lambda < \lambda_c$ with $\eta = 10^{-13}$.

radius on the order of the lattice size. It can be seen from Figure 3 that $\langle R_g^2\rangle$ and $\langle N\rangle$ scale with the lattice size L, with the following scaling exponents:

2d	3d
$\langle R_g\rangle \sim L$	$\langle N\rangle \sim L^{1.30}$
$\langle R_g\rangle \sim L^{0.91}$	$\langle N\rangle \sim L^{1.55}$

which gives, respectively

$$\langle N\rangle \sim \langle R_g\rangle^{1.30} \quad \text{for 2d}$$

$$\langle N\rangle \sim \langle R_g\rangle^{1.70} \quad \text{for 3d} \qquad (15)$$

The exponents from eq 15 can be compared with $1/\nu$ of a SAW: $1/\nu(2d) = 1.33$ and $1/\nu(3d) = 1.69$, which are in a good agreement with our results. This means, that the chains, produced with λ_c in a restricted geometry, are SAWs, as we would have expected. Our results imply, that in a reversible polymerization process, it is possible to control the polymerization index (N), and the size of constructed polymers, by imposing a restricted geometry.

B. The Dilute Regime: $\lambda < \lambda_c$. For $\lambda < \lambda_c$, the system is a dilute solution of polymers, in which the polymer chains do not interact with each other, and they can be treated as single SAWs. Using the analogy between the polydisperse polymer solution and the magnetic system,[12,13] this region is analogous to the high-temperature expansion of the magnetic system, where N is proportional to ϵ^{-1} and the magnetization is proportional to the external magnetic field. By inserting these conditions into eqs 5–7, the following relations are obtained[12,15]

$$\Phi_l = \epsilon^{-\gamma-1}\eta \qquad (16)$$

$$\Phi_p = \epsilon^{-\gamma}\eta \qquad (17)$$

$$\langle N\rangle \sim \epsilon^{-1} \qquad (18)$$

where γ is the free energy critical exponent. Since the chains do not mutually interact, it is sufficient to study a single chain. Therefore, we still keep $\eta = 10^{-13}$, which on the average produces a single chain. Here, however,

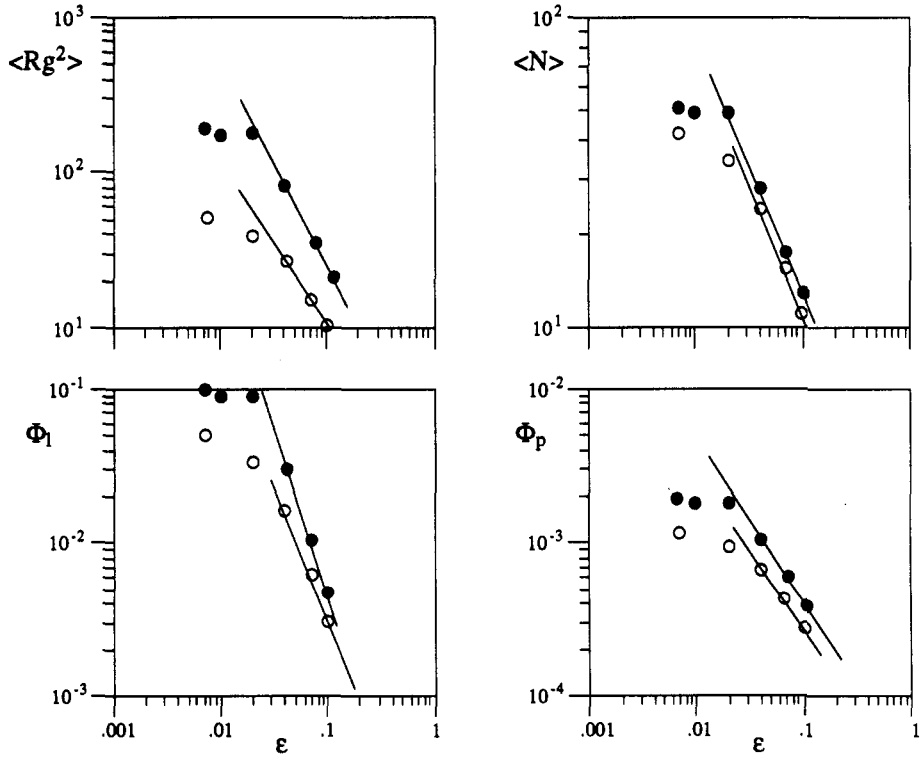

Figure 5. log–log plots of Φ_l, Φ_p, $\langle N\rangle$, and $\langle R_g^2\rangle$ vs ϵ. The filled and open circles denote data for 2d and 3d, respectively. Here $L = 700$ in the square lattice and $L = 100$ in the cubic lattice. $\eta = 10^{-5}$ in both lattices. The slopes which are indicated in each graph, are given in Table 1.

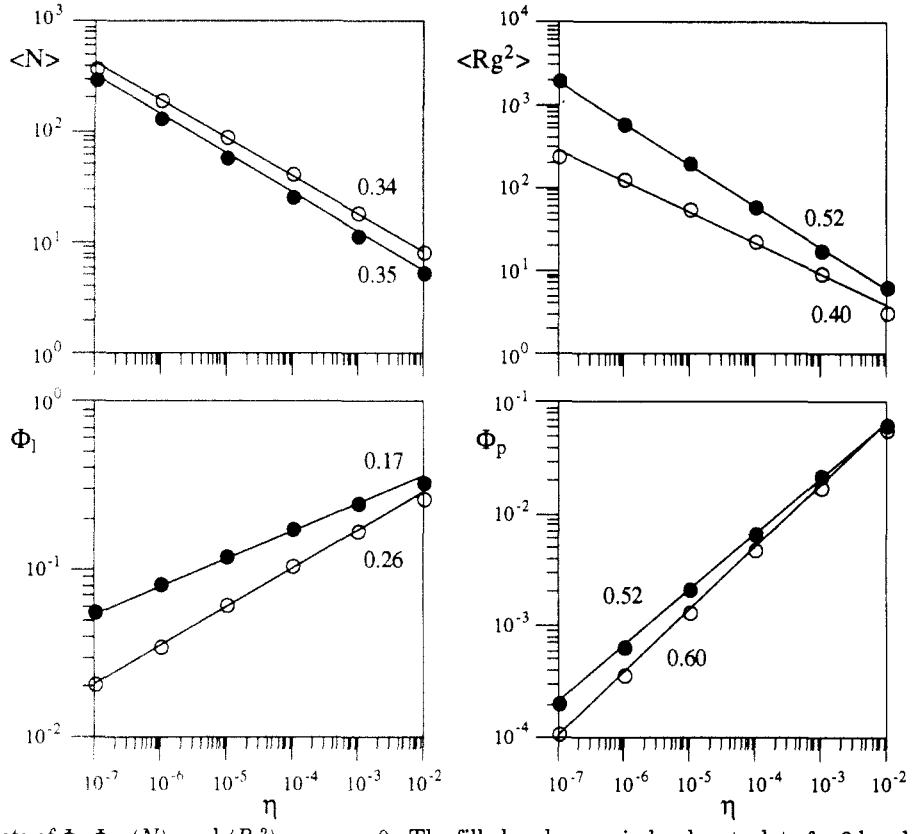

Figure 6. log–log plots of Φ_l, Φ_p, $\langle N\rangle$, and $\langle R_g^2\rangle$ vs η. $\epsilon = 0$. The filled and open circles denote data for 2d and 3d, respectively. The values of $L = 400$ and $\lambda_c = 0.379$ were used in the 2d system, and L = 100 and $\lambda_c = 0.2135$ in the 3d system. The slopes are indicated on the graphs and summarized in Table 2.

Table 1. (a) Slopes of the Graphs Shown in Figure 5 for 2d and 3d and (b) Theoretical Predictions for These Slopes

		$\langle N\rangle$	$\langle R_g^2\rangle$	Φ_l	Φ_p
2d	(a)	−0.85	−1.29	−1.98	−1.07
	(b)	−1	−1.50	−2.34	−1.34
3d	(a)	−0.86	−1.04	−1.81	−0.95
	(b)	−1	−1.18	−2.16	−1.16
theoretical slope relations[a]		−1	-2ν	$-(\gamma+1)$	$-\gamma$

[a] The theoretical slopes listed for (b) were obtained from these relations (see eqs 16–18).

we want the average length, $\langle N\rangle$, of this chain to be determined by λ via ϵ (and not by the lattice limited volume as before). Therefore, we must not use too small an ϵ, for which the lattice boundaries are noticeable. In 2d we can easily use $L = 700$ and a large range for ϵ (from 0.1 to 10^{-4}), but for the 3d lattice, we are limited to $L = 100$. Thus we must use $\epsilon > 0.005$. In Figure 4, the averages $\langle N\rangle$ and $\langle R_g^2\rangle$ are log–log plotted as functions of ϵ. The behavior of $\langle N\rangle \sim \epsilon^{-1}$ is well observed. Therefore, the scaling relation of eq 18 is obeyed for both 2d and 3d lattices. Also, the expected behavior of $\langle R_g^2\rangle \sim \epsilon^{-2\nu}$ is nicely shown, with the known exponents of a SAW [ν(2d) = 0.75 and ν(3d) = 0.588]. Our results confirm the analogy between N^{-1} of an open linear polymer and an ϵ of a critical system. This analogy has been predicted formally, but has never been seen in simulations or experiments until now.

Next, we studied higher values of η, where many polymer chains are constructed. For $\eta = 10^{-5}$, we measured $\langle N\rangle$, $\langle R_g^2\rangle$, Φ_l, and Φ_p as functions of ϵ, and the data are presented in Figure 5. It can be seen from the figure that for small ϵ the graphs reach a plateau, which is the typical behavior of the semidilute regime, where $\langle N\rangle$, $\langle R_g^2\rangle$, Φ_l, and Φ_p are independent of ϵ (the semidilute regime will be further described in section III.C). The reason for the crossover behavior becomes clear if we note the small values of $\langle N\rangle$ in these data ($\langle N < 50$). Since a finite system which does not reach the thermodynamic limit approaches the critical point sooner than a thermodynamically infinite system, the critical region is wider in a finite system. This phenomena is also observed here. That is, the plateaus obtained in each graph of Figure 5 indicate that the system behaves as if it is already at $\epsilon = 0$. The slopes of these graphs are summarized in Table 1. The results show a significant deviation from the expected behavior of a dilute solution, which a pronounced contribution from the semidilute regime. Thus, this region of $\eta > 0$ and $\lambda < \lambda_c$ is a crossover regime between the dilute and the semidilute regimes. This behavior is therefore more noticeable for very small values of ϵ.

In order to obtain the asymptotic values of ν and γ, the system should contain many chains which do not touch each other, and each of these chains should be long enough that the thermodynamic limit is reached. In order to achieve this condition, much larger lattices should be used, which is impractical even with supercomputers.

C. The Semi-Dilute Regime: $\lambda = \lambda_c$ ($\epsilon = 0$). At the transition point, $T = T_c$ and $\epsilon = 0$. Thus, all ϵ dependence should disappear from the relations of eqs 5 and 6, which require $f_p(x) \sim x^{d\nu/\beta}$ and $f_l(x) \sim x^{(d\nu-1)/\beta}$, and give

$$\Phi_l \sim \eta^{(d\nu-1)/2\Delta} \tag{19}$$

$$\Phi_p \sim \eta^{d\nu/2\Delta} \tag{20}$$

$$\langle N\rangle \sim \eta^{-1/2\Delta} \tag{21}$$

where Δ is the gap exponent $\Delta = \gamma + \beta$. Using our SEC procedure, these theoretical relations can be confirmed, and values of critical exponents can be calculated. In Figure 6, we present Φ_l, Φ_p, $\langle N\rangle$, and $\langle R_g^2\rangle$ as functions of η, where $\epsilon = 0$. The slopes of the graphs are summarized

Table 2. Slopes of the Graphs Shown in Figure 6 for 2d and 3d

	$\langle N \rangle$	$\langle R_g^2 \rangle$	Φ_l	Φ_p
2d	−0.35	−0.52	0.17	0.52
3d	−0.34	−0.40	0.26	0.60
theoretical slope relations[a]	$-1/2\Delta$	$-\nu/\Delta$	$(d\nu-1)/2\Delta$	$d\nu/2\Delta$

[a] The theoretical predictionns of eqs 19–21 are denoted. From these slopes, the value of ν and Δ are obtained.

in Table 2, and the following values for ν and Δ are obtained:

$$\nu(2d) = 0.75 \pm 0.01 \qquad \nu(3d) = 0.59 \pm 0.02 \quad (22)$$

$$\Delta(2d) = 1.44 \pm 0.02 \qquad \Delta(3d) = 1.48 \pm 0.02 \quad (23)$$

The values of ν obtained from our simulation are in a good agreement with known values of the SAW model, and we also provide values for the gap exponent Δ. Using a standard scaling relation, other exponents can also be estimated:

	2d	3d
$\beta = d\nu - \Delta$	0.06 ± 0.03	0.29 ± 0.03
$\gamma = \Delta - \beta$	1.38 ± 0.05	1.19 ± 0.05

These results agree well with the known exponents of the SAW model ($\beta(2d) = 0.078$, $\gamma(2d) = 1.3437$[16] and $\beta(3d) = 0.30$, $\gamma(3d) = 1.162$[17]).

An alternative, more "polymeric" representation of the system obtained with λ_c and $\eta > 0$ is to observe the scaling relations of $\langle N \rangle$ and $\langle R_g^2 \rangle$ as functions of the averaged concentration Φ_l. These data are presented in Figure 7, which provide the following scaling relation:

2d	3d
$\langle R_g^2 \rangle \sim \Phi_l^{-2.98}$	$\langle N \rangle \sim \Phi_l^{-1.99}$
$\langle R_g^{2'} \rangle \sim \Phi_l^{-1.49}$	$\langle N \rangle \sim \Phi_l^{-1.25}$

It is interesting to compare our results with the scaling relation derived by de Gennes[18] to described a many chain system at Φ_l^*, the overlap threshold concentration. At this concentration the polymers are just starting to feel each other, thus, Φ_l^* is comparable with the local concentration inside a single polymer and is given by

$$\Phi_l^* \sim \frac{N}{R^d} \sim N^{1-d\nu} \quad (24)$$

from which the following relations are obtained

2d	3d
$R^2 \sim \Phi_l^{*-3}$	$N \sim \Phi_l^{*-2}$
$R^2 \sim \Phi_l^{*-3/2}$	$N \sim \Phi_l^{*-5/4}$

As can be expected, from this comparison we conclude that a reversible growth of polymers with λ_c produces a system at the overlap threshold concentration Φ_l^*, since the chains grow until the point at which they start to overlap. This is consistent with the process of reversible polymerization in a finite box shown before (see Figure 3). There also, the polymers grow until they reach the walls of the box. To best of our knowledge, this is the first time that a system of "blobs" at the overlap threshold concentration has been constructed. Our system reveals a scaling behavior which precisely agrees with the scaling predictions of de Gennes.

D. The Dense Chain Regime: $\lambda > \lambda_c$. We were mainly concerned with the dense chain regime, since it is most controversial and very difficult to simulate. Using our SEC method, we were able to efficiently simulate solutions of up to ≈0.35 link density. Such a high concentration should already reveal the properties of a dense solution, provided that the chains are long enough. Therefore, we can test theoretical predictions for the dense chain limit.

The low temperature limit of the $n \to 0$ vector model corresponds to solutions of high concentration. In this limit, the density of links is not influenced by η. Thus, we should require $f_l(x) \sim$ const. and obtain

$$\Phi_l \sim \epsilon^{(d\nu-1)} \quad (25)$$

The density of polymers should scale like the magnetization. Thus, $f_l(x) \sim x^\delta$ and

$$\Phi_p \sim \epsilon^\beta \eta^{1/2} \quad (26)$$

Therefore,

$$\langle N \rangle \sim \epsilon^{(d\nu-1-\beta)} \eta^{1/2} \quad (27)$$

In order to understand this last relation, let us refer again to de Gennes' description of many chain solutions.[18] For a system of mutually interacting chains, de Gennes defines a correlation length (ξ) as a characteristic length in which a certain part of a polymer chain does not interact with other chains. ξ can be regarded as the average mesh size of the polymer network, and the entire solution consists of blobs of size ξ. Inside a blob the polymer should behave as a SAW, while for distances longer than ξ, the polymer should be ideal. Thus, we expect the scaling relation of

$$\xi \sim g^\nu \quad (28)$$

where g is the number of segments inside a blob. Then

$$\Phi_l = \frac{g}{\xi^d} = g^{(1-d\nu)} \quad (29)$$

Now, if we compare eq 29 with eq 25, which is obtained from the magnetic analogy, we conclude that in the region $T < T_c$

$$g \sim \epsilon^{-1} \quad (30)$$

Therefore, in the dense chain regime, the appropriate analog of ϵ^{-1} is a small portion of the chain g, which scales with ξ of the polymer solution in the same way as the correlation length of the magnetic system scales with ϵ^{-1}. However, we must point out that de Gennes's description for a many chain solution does not consider polydispersity; thus, it is still interesting to see if the same behavior is also observed in our polydisperse system.

According to Gujrati,[13,19] the $n \to 0$ vector model at low temperatures has some singularities which may signal a phase transition line in the $\eta - \lambda$ plane (see Figure 8). If so, the dense polymer phase must be studied directly, without recourse to the magnetic analogy. Gujrati has developed a scaling theory of polydispersity which predicts the existence of an "infinite" chain. This chain appears at η^*, which is defined along the line $\eta^* = \epsilon^{2\Delta}$. Below this line the chains are supposed to be collapsed, and an infinite chain is formed (see Figure 8). Therefore, for $\eta < \eta^*$ the link density Φ_l is composed of two separate contributions: a contribution from the infinite chain

$$\Phi_l^\infty \sim \epsilon^{d\nu-1}\left[1 - \left(\frac{\eta}{\eta^*}\right)^{1/2(1-1/\gamma)}\right] \quad (31)$$

and from finite chains

$$\Phi_l^f \sim \epsilon^{\beta(1+1/\gamma)} \eta^{1/2(1-1/\gamma)} \quad (32)$$

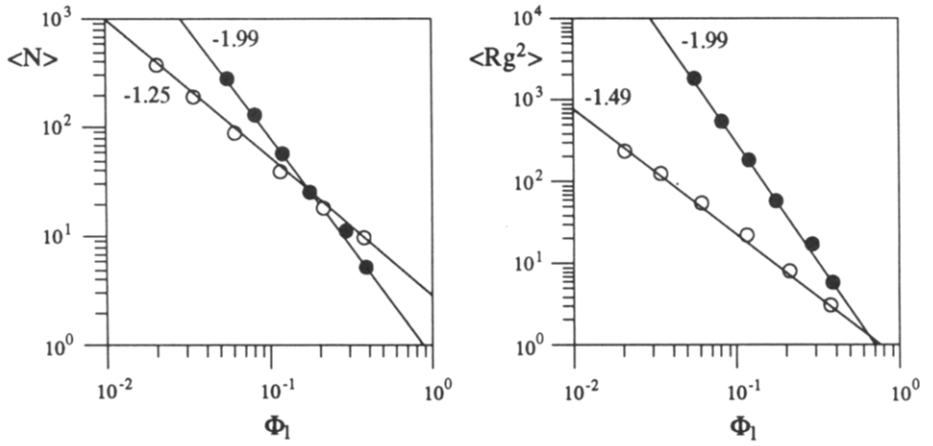

Figure 7. log–log plots of $\langle N \rangle$ and $\langle R_g^2 \rangle$ vs Φ_l. Here, $\epsilon = 0$ and η is in the range 10^{-2}–10^{-6}.

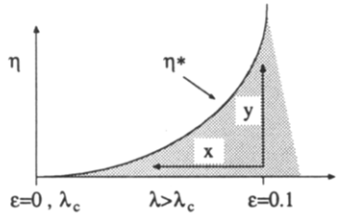

Figure 8. A subsection of the phase diagram of the η–λ plane (according to Gujrati,[13] the line $\eta^* = \epsilon^{2\Delta}$ is indicated). The lines y and x represent measurements with fixed ϵ and fixed η, respectively.

In order to test Gujrati's hypothesis, we also performed the simulation in two regions, below and above the line $\eta^* = \epsilon^{2\Delta}$. The value of the exponent Δ is determined from the results of our simulation in the region $\lambda = \lambda_c$. During the simulation, the longest chain of each configuration was identified, and separate data were collected from those chains. We believe that if there exists an infinite chain, its properties will be revealed from the behavior of the largest chains constructed in the simulation. Typical graphs, which are obtained from simulations in the region $\eta > \eta^*$, are given in Figure 9. It can be seen from the figure that the system's behavior is essentially the same as for the semidilute regime, where Φ_l, Φ_p, and also $\langle N \rangle$ and $\langle R_g^2 \rangle$ are not dependent on ϵ. Therefore, the semidilute regime is actually wider than the Φ_l^* value alone, and contains the entire region above the line $\eta^* = \epsilon^{2\Delta}$. Recall that a similar crossover toward the semidilute regime has also been observed for $\lambda < \lambda_c$, where in Figure 5 the low values of ϵ deviate from straight lines and the curves reach a plateau. This means that the process of formation of chains made of many blobs does not happen at a definite critical value of the concentration, but rather, there is a large range of concentrations in which a polymer chain consists of a single blob and only slightly senses the surrounding chains.

Our results for the region $\eta < \eta^*$, reveal a clearly different behavior from the above. The simplest case is where $\eta \to 0$ and a single chain is constructed. As we have shown previously, for $\lambda < \lambda_c$, the chain is an isolated SAW. If λ is increased above its critical value, the probability of growth is increased (according to eq 9) and overcompensates for the excluded volume restriction of the chain. As a result, the chain grows and fills an increasing number of lattice sites. Therefore, the fractal dimension of the chain will grow accordingly, from d_f of a SAW to 2 of a RW, and finally, for very large values of λ, to 1/d of a collapsed configuration. In this last limit, the chain will cover most of the lattice sites. It should be pointed out, however, that in the 2d case, the fractal dimension of a RW is the same as that of a collapsed chain and is equal to 2. Thus, 2d chains cannot interpenetrate.

In order to characterize this behavior in our system, we measured inner distances, R, along the chain, and plotted them vs N on a log–log scale. The data in Figure 10 indicate a clear transition along the chain, from a swollen SAW configuration to an ideal RW. In comparison, the radius of gyration, R_g^2, is measured over the whole chain and, in the 2d system, shows a crossover exponent between the swollen and the ideal limits. In the 3d case, further increase

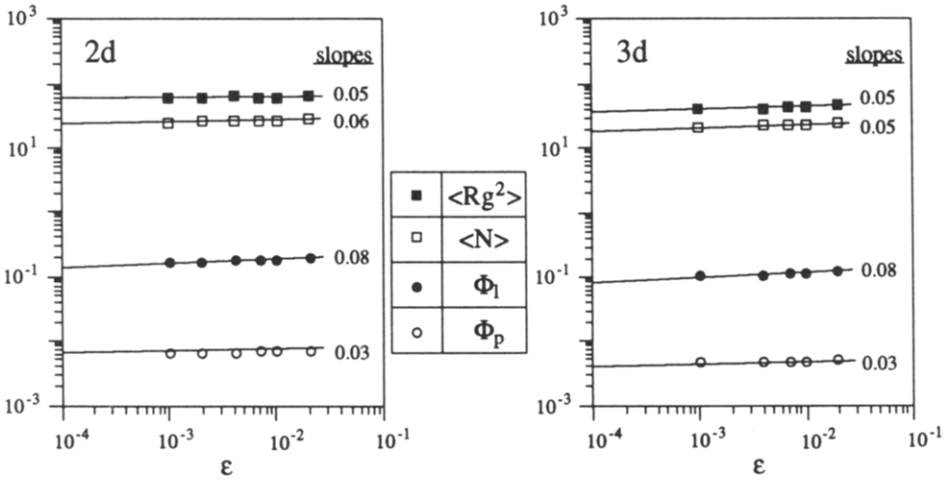

Figure 9. log–log plots of $\langle R_g^2 \rangle$, $\langle N \rangle$, Φ_l, and Φ_p as functions of ϵ. $\eta = 10^{-4}$ in both 2d and 3d systems, and the values of ϵ are chosen to be above the line $\eta^* = \epsilon^{2\Delta}$, thus, $\epsilon < 10^{-2/\Delta}$. The lattice size is $L = 400$ and $L = 50$ for a 2d and a 3d system, respectively.

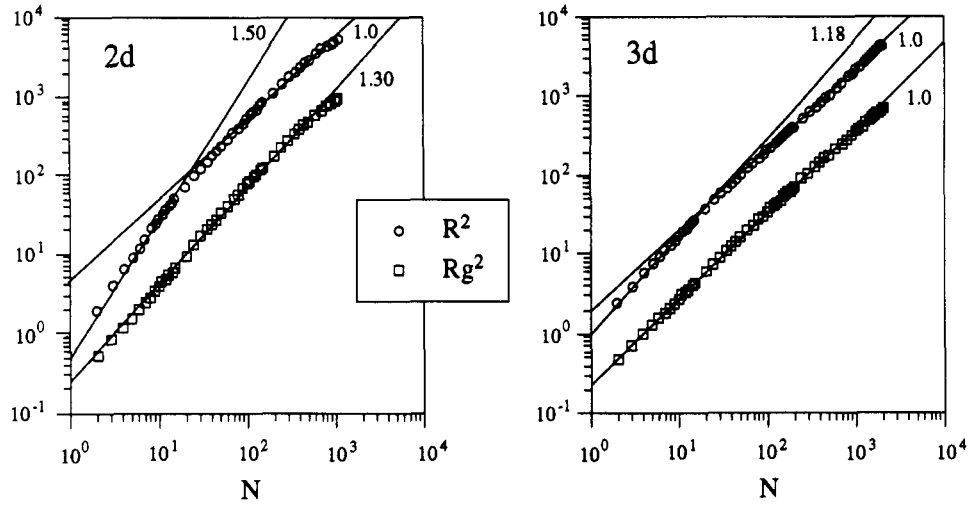

Figure 10. log–log plots of inner distances R^2 and gyration radius R_g^2 as functions of N. $\eta = 10^{-13}$ and $\epsilon = 0.4$ in both 2d and 3d systems, which produce a 2d system of $\Phi_l = 0.29$ and a 3d system of $\Phi_l = 0.35$. The lattice size is $L = 50$ and $L = 20$ for a 2d and a 3d system, respectively.

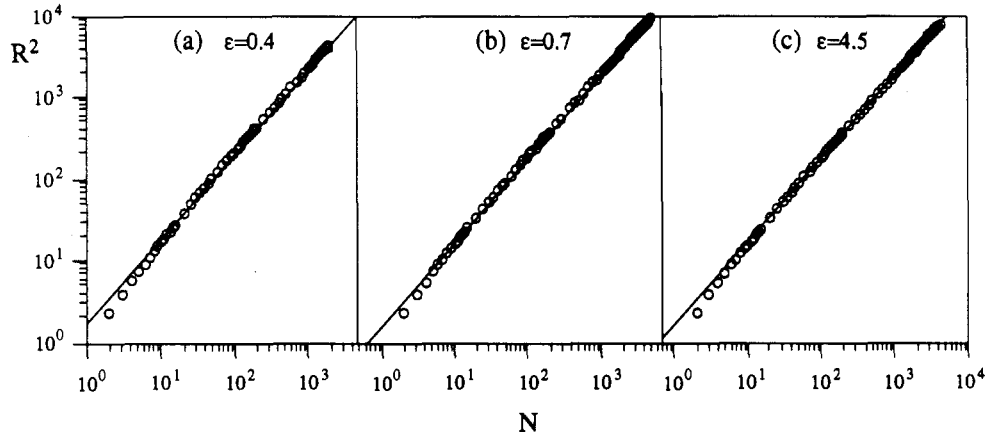

Figure 11. log–log plots of inner distances R^2 as a function of N in a 3d system, with $\eta = 10^{-13}$ and $L = 20$. Under these conditions a single chain is constructed. The slopes of the graphs are all equal to unity; thus, a collapsed configuration is not observed. The parameters of the graphs are (a) $\epsilon = 0.4$, $\lambda = 0.299$, $\Phi_l = 0.365$, $\langle N \rangle = 2900$; (b) $\epsilon = 0.7$, $\lambda = 0.363$, $\Phi_l = 0.485$, $\langle N \rangle = 3880$; (c) $\epsilon = 4.5$, $\lambda = 1.174$, $\Phi_l = 0.664$, $\langle N \rangle = 5300$.

of ϵ should cause the chain to become even more condensed; thus, d_f^{-1} should decrease from $1/2$ to $1/3$. However, in periodic lattice conditions, the end-to-end distance of the chain is measured as if the chain were growing on a bigger lattice. Therefore, as the chain enters the other side of the lattice and starts feeling an excluded volume restriction from its own segments, it causes the chain to become ideal. Thus, although a single chain covers the entire lattice, the system resembles a melt of entangled polymers. This behavior is observed in our simulation. It can be seen from Figure 11 that even for very large values of ϵ, the chain remains ideal and does not collapse. These results should be compared with Mansfield's results for a 3d polydisperse melt of polymers,[20] where $d_f^{-1} = 0.51$ and not $d_f^{-1} = 1/2$, as for an ideal chain. However, his $\langle N \rangle$ was not larger than 512 segments. Thus, we believe that our result for $\langle N \rangle = 1250$, provides a better description of the thermodynamic limit.

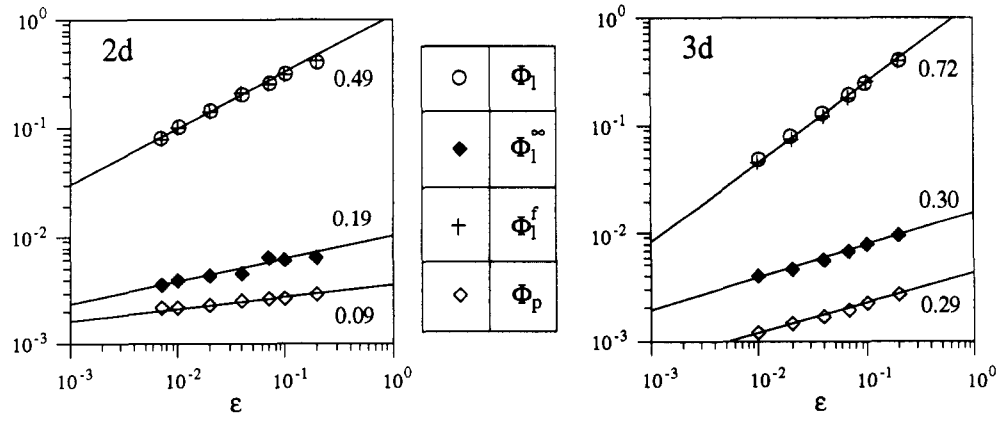

Figure 12. log–log plots of Φ_l, Φ_l^f, Φ_l^∞, and Φ_p as functions of ϵ. $\eta = 10^{-7}$ in both 2d and 3d systems, and the values of ϵ are chosen to be below the line $\eta^* = \epsilon^{2\Delta}$; thus, $\epsilon > 10^{-7/2\Delta}$. The lattice size is $L = 400$ and $L = 40$ for a 2d and a 3d system, respectively.

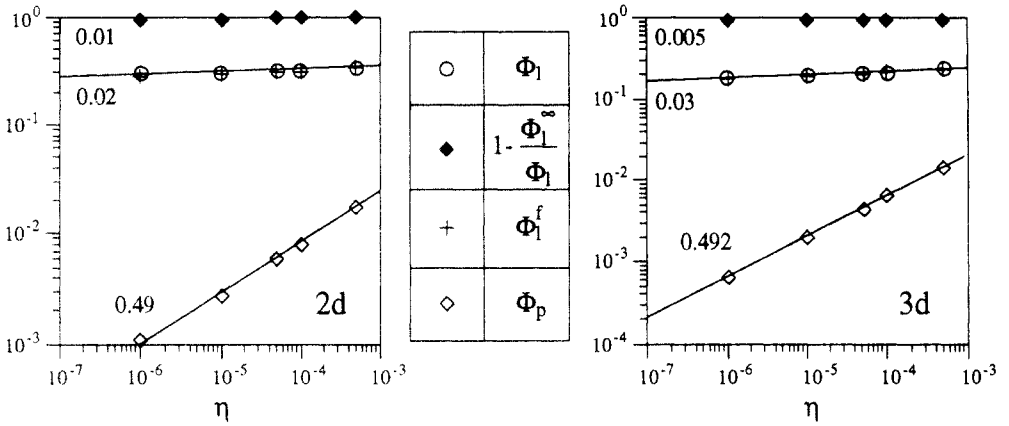

Figure 13. log–log plots of Φ_l, Φ_e^f, $(1 - (\Phi_l^\infty/\Phi_l))$, and Φ_p as functions of η. $\epsilon = 0.1$ in both 2d and 3d systems, for which $\eta^* \approx 10^{-3}$. Thus, a large range of η can be used below the η^* value. The lattice size is $L = 400$ and $L = 40$ for a 2d and 3d system, respectively.

Table 3. (a) Slopes of the Graphs of Figure 12 for 2d and 3d and (b) the Theoretical Predictions for These Slopes

		Φ_l	Φ_l^f	Φ_l^∞	Φ_p
2d	(a)	0.48	0.49	0.19	0.09
	(b)	$^1/_2$	0.136	$^1/_2$	0.08
3d	(a)	0.70	0.72	0.30	0.29
	(b)	0.77	0.56	0.77	0.30
theoretical slope relations[a]		$d\nu - 1$	$\beta(1 + 1/\gamma)$	$d\nu - 1$	β

[a] The theoretical slopes listed for (b) were obtained from these relations (see eqs 25, 26, 31, and 32).

Table 4. (a) Slopes of the Graphs of Figure 13 for 2d and 3d and (b) Theoretical Predictions for These Slopes

		Φ_l	Φ_l^f	$(1 - (\Phi_l^\infty/\Phi_l)$	Φ_p
2d	(a)	0.02	0.01	0.02	0.49
	(b)	0	0.128	0.128	$^1/_2$
3d	(a)	0.03	0.005	0.03	0.49
	(b)	0	0.07	0.07	$^1/_2$
theoretical slope relations[a]		0	$^1/_2(1 - 1/\gamma)$	$^1/_2(1 - 1/\gamma)$	$^1/_2$

[a] The theoretical slopes listed for (b) were obtained from these relations (see eqs 25, 26, 32, and 33).

The following step was to search for a collapsed phase above $\eta = 0$, where more than a single chain is constructed. In this region, we were also interested in confirming eqs 25–27 and testing Gujrati's predictions of eqs 31 and 32. In order to study the ϵ dependence of the density of links and of polymers, η was kept fixed and ϵ was varied but kept below the line $\eta^* = \epsilon^{2\Delta}$ (see path x in Figure 8). Since η^* varies as ϵ^3, there is only a limited number of ϵ values which can be studied.

In Figure 12 we present the data from a study performed along the x path (Figure 8). Results from the slopes of the graphs and comparison with eqs 25, 26, 31, and 32 are summarized in Table 3. Although only a limited number of ϵ values could be used in this region, our results for Φ_l and Φ_p are in a reasonable agreement with the values of a SAW, which are to be expected from the $n = 0$ vector model. From Table 3 we also see that the slopes obtained for Φ_l^f and Φ_l^∞ as functions of ϵ are far from those predicted by Gujrati. Therefore we conclude that finite chains, not an infinite chain, if one exists at all, dictate the behavior of Φ_l.

The other direction of study is along the y path of the phase diagram (see Figure 8), where ϵ is kept fixed and η is varied. The η dependence of Φ_l^∞ cannot be shown directly from eq 31; thus, we divide eq 31 by eq 25, in order to study the following relation:

$$1 - \frac{\Phi_l^\infty}{\Phi_l} \sim \eta^{1/2(1-1/\gamma)} \tag{33}$$

The results are presented in Figure 13 and the slopes of the graphs are summarized in Table 4, together with the theoretical predictions. The agreement is good for Φ_l and Φ_p. As for Φ_l^f and $(1 - (\Phi_l^\infty/\Phi_l))$, since the value of $^1/_2(1 - 1/\gamma)$ is very close to zero (in both 2d and 3d systems), Gujrati's prediction could not be ruled out in this case.

In addition to the results for the concentrations, the average chain length $\langle N \rangle$ was also measured and presented

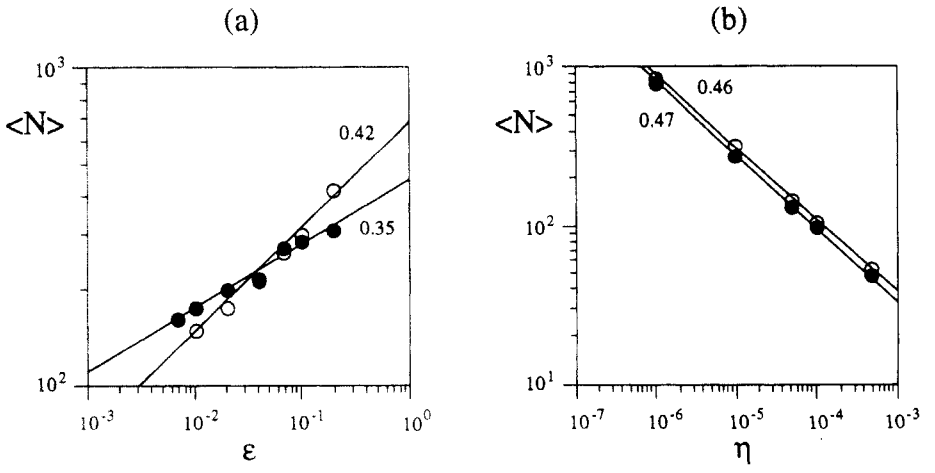

Figure 14. log–log plots of $\langle N \rangle$ (a) as a function of ϵ with $\eta = 10^{-5}$ and (b) as a function of η with $\epsilon = 0.1$. The filled and open circles denote data for 2d and 3d, respectively.

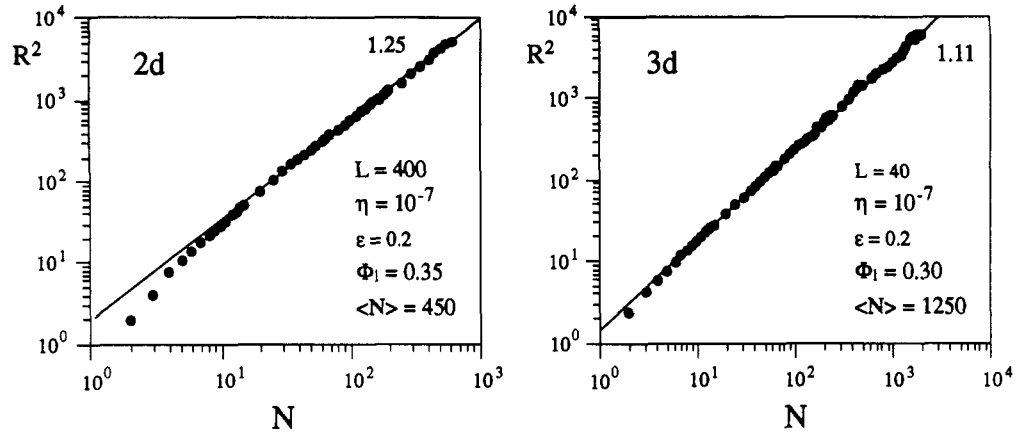

Figure 15. log-log plots of inner distances R^2 as a function of N. The simulation parameters, the resulting link density, and $\langle N \rangle$ are denoted on the figure.

in Figure 14. The slopes from the graphs of Figure 14 should be compared with the theoretical predictions of eq 27. From Figure 14b the expected slope of $^1/_2$ is approximately obtained in both 2d and 3d systems. The data of Figure 14a deviate slightly from straight lines, which causes large error bars in our slopes:

$$d\nu - 1 - \beta = \begin{cases} 0.35 \pm 0.1 & 2d \\ 0.42 \pm 0.1 & 3d \end{cases} \quad (34)$$

The results of eq 34 should be compared with the ν and β of a SAW,

$$d\nu - 1 - \beta = \begin{cases} 2{\cdot}0.75 - 1 - 0.08 = 0.42 & 2d \\ 3{\cdot}0.59 - 1 - 0.30 = 0.47 & 3d \end{cases} \quad (35)$$

which are within the limits of our results for eq 34.

A more direct test for the existence of a collapsed phase is to measure inner distances along the chains and calculate their fractal dimensions. We have performed several measurements in this dense chain region, without any evidence for fractal dimensions smaller than 2 (which characterize the ideal behavior of a RW). On the contrary, in most cases, a crossover between a swollen chain and an ideal chain is observed. In Figure 15, examples of highly concentrated solutions are presented, with a large $\langle N \rangle$, which should characterize a dense system in both 2d and 3d systems. From the slopes of the graphs we obtain

$$d_f(2d) = 1.6 \pm 0.02 \qquad d_f(3d) = 1.8 \pm 0.02 \quad (36)$$

These fractal dimensions are significantly smaller than even those of an ideal chain and therefore certainly cannot imply a collapsed configuration.

From all the results which we obtained from the region below the line $\eta^* = \epsilon^{2\Delta}$, we can conclude that this region represents a polydisperse solution in the *semidilute* region. We observed a crossover to the region of a melt of chains only for very large ϵ and small η.

IV. Conclusions

Highly concentrated solutions are very difficult to simulate because of the long relaxation time of the entangled polymers (a slowing down effect). Our SEC simulation method provides an uncorrelated configuration after N^2 MC moves, which is at least N times faster than most other simulation techniques and has the same efficiency as the slithering-snake[21] and the Berretti and Sokal[8] methods. However, unlike the slithering-snake process which can be entrapped in a dead-end position, our SEC process is ergodic. Also, SEC is an especially efficient method for studying polymer solutions, while the Berretti and Sokal method was not extended to study systems other than a single SAW.

As a result of this efficiency, our method can provide a large number of equilibrium configurations from any unequilibrated starting configuration and allows us to simulate a large range of concentration values. In comparison, most other simulation techniques[22] must start from an equilibrium configuration and can measure a limited number of configurations around the starting one. This might not influence measurements of dynamical properties, but can certainly influence measurements of equilibrium properties.

Our SEC method is a stepwise elongation and contraction process, which is controlled by two fugacities: λ for a polymer link and η for the number of polymers in the solution. In the region of $\eta \to 0$ and $\lambda < \lambda_c$, we have confirmed the swollen SAW configuration, where we measured $R \sim N^{1/d_f}$ with d_f of a SAW in 2d and 3d systems. Scaling measurements as functions of ϵ showed exactly the same scaling behavior as with $\langle N \rangle^{-1}$, which confirmed the correspondence $\epsilon \leftrightarrow N^{-1}$. Until now, the analogy between a polymer system and the $n \to 0$ vector model has only been predicted formally, but has never been seen in simulations or experiments. In this regime, we also studied the effect of a finite size lattice on the configuration of the chains. We found that the number of segments of the polymers can be exactly controlled, using a restricted geometry.

At $\lambda = \lambda_c$, the polymers grow until the point at which they start to overlap. This is because λ_c is only compensating for the excluded volume restriction of the polymer itself, and not of surrounding chains. As a result, we found that the threshold concentration Φ_l^* is obtained with a remarkable precision. The concept of Φ_l^* was used by de Gennes in order to develop his "blob" representation for a *monodisperse* polymer solution. Therefore, our results indicate that this blob picture provides a suitable description of the overlap threshold concentration regime of a *polydisperse* system, as well. Moreover, we observed that Φ_l^* describes a large range of concentrations, each one of which can be viewed as a crossover regime, from the single SAW to the semidilute regime, where a chain is represented by a sequence of blobs.

For $\lambda > \lambda_c$, a large range of concentrations and chain lengths were studied. We were mainly interested in the controversial issue of whether there exists a collapsed phase below the line $\eta^* = \epsilon^{2\Delta}$, as was claimed by Gujrati,[13,19] on the basis of the following argument. As η is lowered, Φ_p is reduced to zero, and the length of each chain should grow in order that the total density of links will not change

(since it does not depend on η). Gujrati claims that only the mechanism of two chain ends aggregating can achieve these conditions. Since the probability for this mechanism is very low, and it is even lower if the chains are interpenetrating, he concludes that the chains must be separated, and as a result, they should have a collapsed configuration. The existence of a collapsed phase, however, is not favorable from the entropic point of view. Our SEC process provides an alternative mechanism to that suggested by Gujrati. The growth of the chains does not require aggregation of chains and is not influenced by the interpenetration of chains. Thus, the assumption of a collapsed transition can be avoided.

Indeed, in our simulation we found no evidence for a collapsed phase. In fact, our results for d_f are a little higher than those of a swollenn SAW. In an additional search for a collapsed chain, where we calculated inner distances in a polymer in order to measure the fractal dimension of the chain, we found a d_f of a SAW for short distances and a d_f of an ideal random walk for long distances (which equaled 2). Again there was no evidence for a collapsed phase.

Acknowledgment. I would like to thank Zeev Alexandrowicz for suggesting the subject to me and for fruitful discussions.

References and Notes

(1) Szwarc, M.; Levy, M.; Milkovitch, R. *J. Am. Chem. Soc.* **1956**, *78*, 2656. Szwarc, M. *Carbanions, Living Polymers and Electron Transfer Processes*; Wiley: New York, 1968.

(2) Safran, S. A.; Turkevich, L. A.; Pincus, P. *J. Phys. (Paris)* **1984**, *45*, L–69.

(3) Oosawa, F.; Asakura, S.; Hotta, K.; Imai, N.; Ooi, T. *J. Polym. Sci.*, **1959** *37*, 323; Gskin, F.; Cantor, C. R.; Shelansky, M. L. *J. Mol. Biol.* **1974**, *89*, 737.

(4) de Gennes, P. G. *Phys. Lett.* **1972**, *38A*, 399.

(5) des Cloizeaux, J. *J. Phys. (Paris)* **1975**, *36*, 281.

(6) Gujrati, P. D. *Phys. Rev. B* **1985**, *31*, 4375.

(7) Wheeler, J. C.; Stilck, J. F.; Petschek, R. G.; Pfeuty, P. *Phys. Rev. B* **1987**, *35*, 284.

(8) Berretti, A.; Sokal, A. *J. Stat. Phys.* **1985**, *40*, 483.

(9) Schäfer, L.; Witten, T. A. *J. Phys. (Paris)* **1980**, *41*, 459; Knoll, L.; Schäfer, L.; Witten, T. A. *J. Phys. (Paris)* **1981**, *42*, 767.

(10) Wheeler, J. C.; Petschek, R. G. *Phys. Rev. B* **1992**, *45*, 171.

(11) Alexandrowicz, Z. *Physica A* **1990**, *167*, 507.

(12) Gujrati, P. D. *Phys. Rev. A* **1981**, *24*, 2096.

(13) Gujrati, P. D. *Phys. Rev. Lett.* **1985**, *55*, 1161.

(14) Stauffer, D. *Phys. Rep.* **1979**, *54*, 1.

(15) Petschek, R. G.; Pfeuty, P.; Wheeler, J. C. *Phys. Rev. A* **1986**, *34*, 2391.

(16) Saleur, H. *Phys. Rev. B* **1987**, *35*, 3657.

(17) LeGuillou, J. C.; Zinn-Justin, J. *Phys. Rev. B* **1980**, *21*, 3976; *J. Phys. (Paris)* **1987**, *48*, 19.

(18) de Gennes, P. G. *Scaling Concepts in Polymer Physics*; (Cornell University Press: Ithaca, NY, 1979.

(19) Gujrati, P. D. *Phys. Rev. B* **1989**, *40*, 5140.

(20) Mansfield, M. L. *J. Chem. Phys.* **1982**, *77*, 1554.

(21) Kron, A. K.; Ptitsyn, O. B.; Skvortsov, A. M.; Fedorov, A. K. *Mol. Biol.* **1967**, *1*, 487; Wall, F. T.; Mandel, F. *J. Chem. Phys.* **1975**, *63*, 4592.

(22) Kremer, K.; Binder, K. *Comput. Phys. Rep.* **1988**, *7* (6), 259; and references therein.